

Wind Loads on Skillion and Lean-To Roof Buildings

Joshua Eaton¹, Prof. John Ginger²

¹joshua.eaton@my.jcu.edu.au

²john.ginger@jcu.edu.au

ABSTRACT

Houses with skillion and lean-to roof profiles are popular throughout Australia. However, Australian Standards AS/NZS 1170.2 and AS 4055 do not provide wind design data specifically for this roof shape. Currently, engineers and builders use data for hip, gable, and mono-slope roofs in the standards to design skillion roofs. Wind tunnel tests were carried out simulating a 1/50 scale skillion model within a suburban environment to obtain design wind loads on the roof, walls, and rise of the house. The rise experienced large positive pressures that coincide with the largest suction pressures occurring on the corner region of the rise eave. This was due to the wind flow separation over the rise causing a formation of vortices on the top of the eave. The aerodynamic shape factors (C_{fig}) found for these regions were larger than the values provided by AS/NZS 1170.2 on roof slopes.

1. Introduction

Skillion and lean-to roofs are a popular roof shape for Australian housing, designed to comply with AS/NZS 1170.2 (2011) and AS 4055 (2012). However, these standards only provide wind loading data for rectangular-plan hip, gable, and mono-slope roof buildings. In Australia, wind storms are the most destructive weather phenomena to impact housing. The roof is the critical part of the house experiencing the largest suction pressures, making it the most vulnerable to failure. It is imperative to provide reliable wind load design data, otherwise the structural integrity of the house can be compromised and potentially lead to significant damages.

Skillion and lean-to roof configurations consist of two sloped roofs connected by an upright section known as the rise, as shown in Figures 1 and 2. These roofs are designed to allow the natural flow of air and light into the building with high sloped roofs providing the opportunity for clerestory windows and skylights.



Figure 1: Skillion and lean-to roof houses

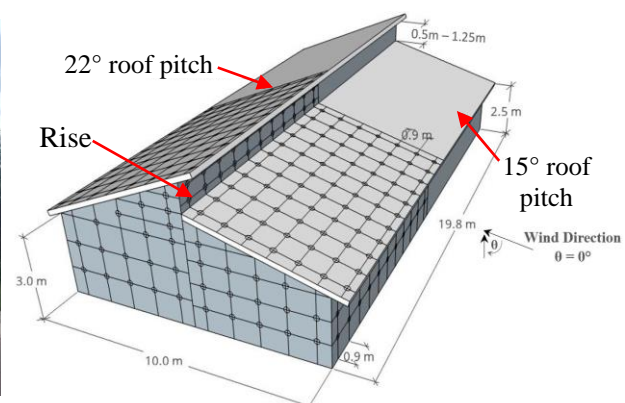


Figure 2: Typical skillion roof building tested

Previous studies have focused on low-rise rectangular shaped hip and gable roof buildings, sawtooth and mono-slope roofs, square plan pyramidal roofs, and stepped roofs. These studies show how various roof slopes and ridge configurations affect the wind pressure distribution and influence regions experiencing the largest pressures. The geometry of rectangular hip and gable roof buildings allows the wind to flow up and over the roof ridge with minimal obstruction. Whereas, a skillion and lean-to roof includes the rise area between slopes which effectively acts as an obstacle for the wind and can significantly alter flow and influence pressures across the roof.

The formation of vortices generates large suction pressures at the windward corners, ridges, and leading edges on the buildings' roof. Most of the damage to roofing elements have been caused by large fluctuating uplift forces in these regions. Studies have shown many occurrences of structural failures associated with insufficient construction and incorrect design loads, thus raising the importance of accurate wind design information for skillion roofs. The failure to incorporate accurate wind load design data can result in significant damage as seen in Figure 3.



Figure 3: Wind damage to skillion roof buildings

As the demand for these roof profiles continues to increase, so does the importance of optimal design wind load data. This study aims to obtain external pressures on the roof, walls, and rise of typical skillion roof shapes to address the lack of data on this type of building, as detailed in Eaton (2020).

2. Testing and Analysis

Tests were conducted in the Atmospheric Boundary Layer Wind Tunnel at the Cyclone Testing Station, James Cook University. A typical 10m x 19.8m x 3m skillion and lean-to roof building shown in Figure 2 was constructed at a length scale of 1/50. The approach wind flow was simulated as a suburban Terrain Category 3 using an array of 50mm tall blocks placed on the floor upwind of the model. 252 pressure taps were installed in a grid pattern representative of 900mm batten and truss spacing, and 600mm eave overhang. The two roof slopes are 22° and 15°. The model to prototype velocity scale is 1/2.5 and time scale is 1/20. Therefore, 30 seconds in model scale is equivalent to 10 minutes in full scale.

Analysis of the current housing industry showed typical rise heights within the range of 0.5m to 1.25m. Figures 4 and 5 show the experimental setup at wind direction (θ) of 0°, and the four rise heights tested.

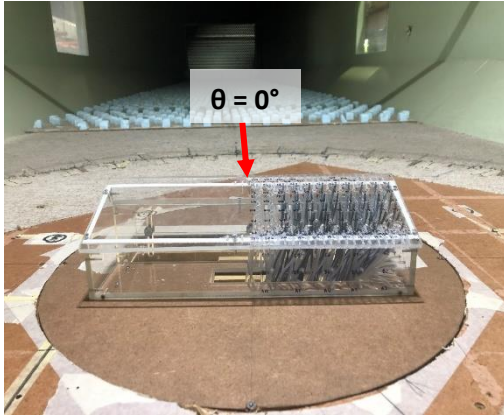


Figure 4: Wind tunnel testing setup

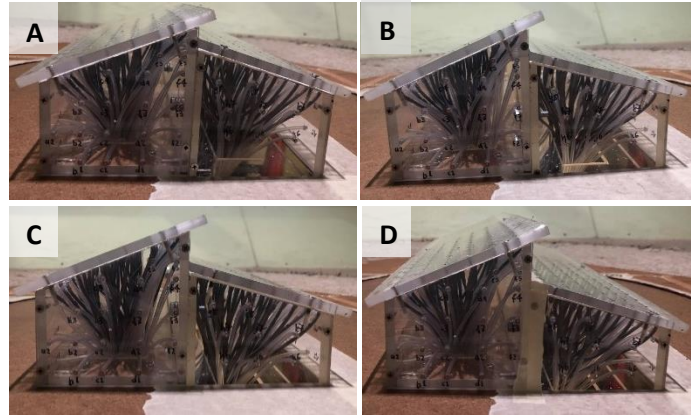


Figure 5: Model rise heights – A:0.5m, B:0.75m, C:1m, D:1.25m

The pressure taps were connected to transducers which record external pressures on the model surface with a sampling frequency of 500 Hz. This time varying pressure data is analysed to calculate pressure coefficients varying with time (t) as: $C_p(t) = p(t) / \left(\frac{1}{2} \rho \bar{U}_h^2 \right)$, where $\frac{1}{2} \rho \bar{U}_h^2$ is the mean dynamic pressure at the building mid-roof height of 4m. The aerodynamic shape factor, $C_{fig} = C_{p_{peak}} / G_u^2$ consistent with AS/NZS 1170.2 is found from the peak pressure coefficient and velocity gust factor, $G_u = 1.96$.

3. Results and Discussion

Data for the 1m rise height configuration shown in Figure 5C has been used to present the pressure coefficient and aerodynamic shape factor results in the following figures.

3.1 Pressure Coefficient, C_p

Figure 6 shows the mean C_p values for a wind direction (θ) of 0° , demonstrating the effects of the skillion roof geometry on the wind flow and corresponding pressure regions. Positive pressures are experienced on the windward wall, upwind slope, and rise area. Negative pressures are occurring on the downwind slope and leeward wall. AS/NZS 1170.2 provides negative pressure coefficients for upwind roof slopes as suction pressures typically occur on hip, gable, or mono-slope roofs. However, Figure 6 shows the majority of the skillion upwind slope (B) experiences positive pressures that are not accounted for in wind design standards. The largest positive pressures are found on the underside of the rise eave. This is due to the increase in velocity as the wind travels up the roof and impacts the rise, forcing the wind to continue its motion acting upwards into the eave resulting in large positive pressures.

Figure 7 shows the mean C_p values for $\theta = 90^\circ$. Negative pressures occur throughout the roof and sidewalls. As the wind encounters flow separation over the skillion roof edges, distinct pressure regions can be identified with the largest suction pressures occurring at the leading edges. However, in Figure 6, the leading edges of the upwind slope (B) show minimal negative pressures. This shows the rise area slows the wind speed and reduces the effect of eddy's and vortices on the leading edges.

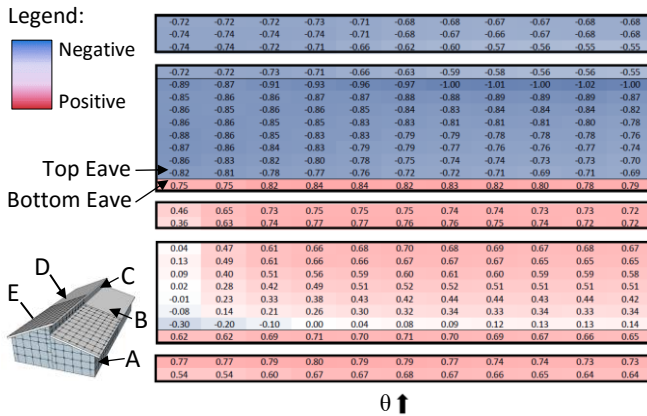


Figure 6: Mean C_p distribution for $\theta = 0^\circ$



Figure 7: Mean C_p distribution for $\theta = 90^\circ$

Figures 8 and 9 show the variation in pressure on the rise and corner of the rise eave as the wind direction changes. In Figure 8 the corner of the rise eave experiences peak negative pressures at $\theta = 50^\circ$. This corresponds with the largest positive pressures occurring on the rise as shown in Figure 9.

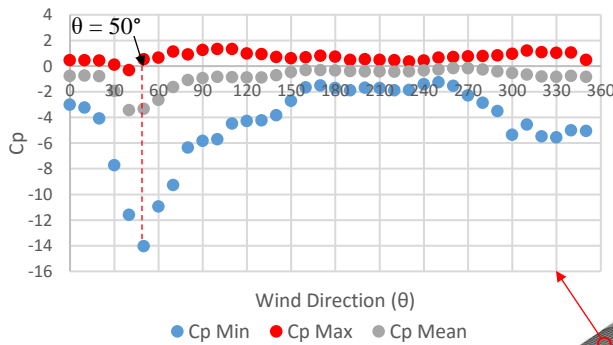


Figure 8: C_p for top rise eave tap

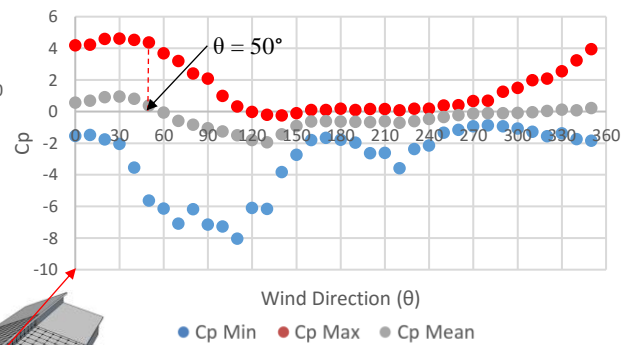
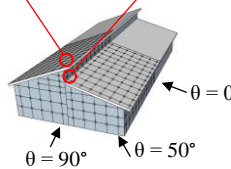


Figure 9: C_p for rise tap



3.2 Aerodynamic shape factor, C_{fig}

To relate the skillion roof results to AS/NZS 1170.2 and AS 4055, the C_{fig} pressure maps can be compared to values from the Australian Standards for hip, gable, and mono-slope roofs, identifying the major differences. Figure 10 displays the positive C_{fig} values for $\theta = 0^\circ \pm 45^\circ$, and Figure 11 shows the negative C_{fig} values for $\theta = 90^\circ \pm 45^\circ$.

As the rise is an upright section between roofs, the pressures are compared to a wall, showing the rise to experience substantially larger positive and negative pressures in Figures 10 and 11. For $\theta = 0^\circ \pm 45^\circ$ the most accurate design C_{fig} data for the rise is the AS/NZS 1170.2 windward wall value of +1.05 in a K_L region of 1.5. However, Figure 10 shows the rise area experiences a larger positive C_{fig} of +1.49. These larger pressures are caused by the impact of wind with a greater velocity as the wind travels up the roof slope. A similar trend is shown in Figure 11, with a peak negative C_{fig} for the rise of -1.76, as opposed to AS/NZS 1170.2 providing a smaller sidewall C_{fig} value of -1.3 for a K_L region of 2.0.

AS/NZS 1170.2 provides negative C_{fig} values for the design of hip, gable, and mono-slope roofs. For $\theta = 0^\circ \pm 45^\circ$ in Figure 10, the wind flow obstruction from the rise area dramatically reduces the wind speed in this region and generates positive pressures on the upwind roof slope.

In Figure 11, the region containing the largest suction pressures is found at the leading edges of the building due to the wind flow separation causing a formation of vortices. The corner of the rise eave is shown to experience the critical suction pressures on the skillion building with a C_{fig} value of -3.8.

Compared to the design information for hip, gable, and mono-slope crosswind roofs, AS/NZS 1170.2 provides a smaller C_{fig} value of -2.7 for a corner K_L 3.0 region.

0.34	0.34	0.28	0.22	0.20	0.17	0.13	0.10	0.10	0.11	0.11
0.11	0.11	0.13	0.14	0.14	0.13	0.13	0.13	0.13	0.12	0.12
0.11	0.11	0.11	0.11	0.12	0.13	0.11	0.08	0.09	0.10	0.10
0.34	0.34	0.29	0.31	0.25	0.31	0.27	0.23	0.36	0.25	0.14
0.27	0.21	0.22	0.22	0.25	0.21	0.24	0.32	0.32	0.26	0.14
0.23	0.21	0.19	0.25	0.33	0.25	0.27	0.26	0.26	0.31	0.18
0.21	0.20	0.25	0.25	0.31	0.27	0.23	0.24	0.23	0.42	0.19
0.25	0.19	0.23	0.28	0.26	0.27	0.26	0.21	0.15	0.20	0.09
0.25	0.20	0.35	0.30	0.22	0.18	0.20	0.15	0.21	0.19	0.09
0.24	0.17	0.23	0.21	0.19	0.22	0.13	0.17	0.17	0.20	0.11
0.30	0.24	0.25	0.22	0.21	0.23	0.20	0.21	0.23	0.18	0.10
0.37	0.37	0.28	0.26	0.31	0.26	0.30	0.21	0.32	0.27	0.10
1.46	1.46	1.38	1.20	1.24	1.16	1.15	1.14	1.19	1.20	0.98
1.49	1.35	1.15	1.11	1.09	1.05	1.15	1.03	1.07	1.06	0.88
1.26	1.23	1.09	1.03	0.98	0.97	1.03	1.00	0.99	0.99	0.85
0.97	1.06	1.05	0.95	0.97	0.94	0.97	0.94	0.96	0.70	0.76
0.85	0.87	0.89	0.84	0.82	0.86	0.83	0.81	0.83	0.71	0.70
0.67	0.72	0.71	0.72	0.72	0.71	0.73	0.73	0.71	0.65	0.65
0.63	0.65	0.61	0.62	0.64	0.64	0.67	0.64	0.67	0.60	0.58
0.58	0.59	0.58	0.59	0.59	0.59	0.65	0.59	0.60	0.55	0.53
0.56	0.59	0.57	0.56	0.60	0.60	0.62	0.65	0.66	0.53	0.54
0.90	0.83	0.75	0.73	0.73	0.75	0.71	0.69	0.73	0.58	0.55
1.07	1.07	0.98	0.96	0.95	0.95	0.94	0.93	0.88	0.84	0.82
0.98	0.98	0.95	0.91	0.90	0.89	0.86	0.83	0.84	0.85	0.85
0.78	0.78	0.78	0.77	0.74	0.71	0.71	0.71	0.68	0.64	0.64

$\theta \uparrow$

Figure 10: Positive C_{fig} for $\theta = 0^\circ \pm 45^\circ$

-0.76	-0.76	-0.76	-0.75	-0.62	-0.50	-0.52	-0.54	-0.57	-0.60	-0.60
-0.87	-0.87	-0.75	-0.64	-0.55	-0.46	-0.46	-0.45	-0.46	-0.47	-0.47
-0.83	-0.83	-0.83	-0.83	-0.75	-0.66	-0.59	-0.51	-0.50	-0.48	-0.48
-1.21	-1.21	-0.88	-0.89	-0.71	-0.62	-0.58	-0.53	-0.52	-0.51	-0.41
-1.79	-1.42	-1.39	-1.19	-0.96	-0.92	-0.87	-0.82	-0.85	-0.78	-0.63
-2.07	-1.49	-1.35	-1.02	-0.95	-1.00	-0.86	-0.76	-0.72	-0.78	-0.73
-1.92	-1.63	-1.29	-1.06	-1.04	-0.91	-0.83	-0.80	-0.96	-1.07	-0.83
-1.92	-1.69	-1.27	-1.15	-1.04	-0.99	-1.03	-1.03	-1.17	-1.26	-1.09
-2.06	-1.52	-1.30	-1.26	-1.32	-1.27	-1.22	-1.34	-1.36	-1.42	-1.12
-1.80	-1.60	-1.50	-1.60	-1.63	-1.76	-1.99	-1.73	-1.58	-1.51	-1.33
-2.12	-1.90	-2.61	-2.46	-2.34	-2.35	-1.97	-1.72	-1.57	-1.47	-1.17
-3.39	-3.84	-2.73	-2.21	-2.00	-1.70	-1.65	-1.31	-1.37	-1.28	-1.25
-1.74	-1.74	-1.53	-1.30	-1.27	-1.11	-0.94	-0.87	-0.76	-0.64	-0.55
-1.53	-1.76	-1.40	-1.16	-0.93	-0.89	-0.76	-0.62	-0.61	-0.61	-0.54
-1.48	-1.46	-1.12	-0.97	-0.96	-0.87	-0.79	-0.73	-0.69	-0.63	-0.55
-1.63	-1.54	-1.18	-1.06	-1.01	-0.93	-0.89	-0.83	-0.83	-0.58	-0.62
-2.30	-1.64	-1.21	-1.15	-1.08	-1.02	-0.97	-0.91	-0.95	-0.78	-0.70
-1.71	-1.58	-1.18	-1.05	-1.06	-1.08	-0.91	-0.99	-0.95	-0.80	-0.81
-1.87	-1.44	-1.13	-1.03	-0.87	-0.89	-0.87	-0.87	-0.92	-0.81	-0.75
-1.79	-1.33	-1.06	-0.95	-0.82	-0.85	-0.75	-0.78	-0.81	-0.77	-0.80
-2.09	-1.26	-1.08	-0.95	-0.85	-0.76	-0.67	-0.78	-0.80	-0.76	-0.64
-1.52	-1.40	-1.33	-1.07	-1.15	-0.88	-0.77	-0.77	-0.74	-0.61	-0.76
-1.09	-1.09	-0.88	-0.78	-0.69	-0.67	-0.57	-0.55	-0.51	-0.35	-0.33
-0.67	-0.67	-0.63	-0.59	-0.53	-0.47	-0.44	-0.41	-0.38	-0.35	-0.35
-0.66	-0.66	-0.57	-0.48	-0.45	-0.41	-0.41	-0.40	-0.38	-0.36	-0.36

$\theta \rightarrow$

Figure 11: Negative C_{fig} for $\theta = 90^\circ \pm 45^\circ$

Additional analysis was conducted on the rise, altering the rise height within a range of 0.5m to 1.25m. The black dotted outline in Figure 10 shows the region focused on in Figure 12 for the comparison of the four rise height configurations. This figure uses the positive C_{fig} results for $\theta = 0^\circ \pm 45^\circ$ to demonstrate the effects of an increased rise height on the corresponding pressures. Comparing the peak pressures observed on the four rise height variations, Figure 12 shows as the height is increased, the pressure increases due to channeling of the wind to the larger area.

0.20	0.19	0.37	0.31	0.24	0.26	0.28	0.24	0.25	0.20	0.35	0.30	0.29	0.19	0.47	0.35
0.26	0.20	0.26	0.26	0.28	0.35	0.28	0.25	0.24	0.17	0.23	0.21	0.27	0.24	0.40	0.32
0.39	0.43	0.26	0.26	0.31	0.26	0.21	0.24	0.30	0.24	0.25	0.22	0.36	0.33	0.29	0.25
0.33	0.33	0.28	0.28	0.36	0.28	0.29	0.36	0.37	0.37	0.28	0.26	0.60	0.39	0.32	0.30
1.29	1.29	1.36	1.35	1.30	1.30	1.40	1.26	1.46	1.46	1.38	1.20	1.56	1.56	1.55	1.37
1.29	1.16	1.18	1.13	1.21	1.22	1.26	1.18	1.49	1.35	1.15	1.11	1.41	1.51	1.38	1.20
1.26	1.23	1.09	1.03	1.26	1.23	1.09	1.03	1.26	1.23	1.09	1.03	1.24	1.41	1.29	1.12
0.99	1.07	1.08	1.02	1.00	1.15	1.08	1.07	0.97	1.06	1.05	0.95	1.00	1.21	1.22	1.11
0.73	0.85	0.87	0.89	0.73	0.80	0.83	0.83	0.85	0.87	0.89	0.84	0.83	0.96	0.97	1.00
0.60	0.69	0.67	0.70	0.66	0.61	0.64	0.71	0.67	0.72	0.71	0.72	0.65	0.77	0.83	0.80
0.58	0.57	0.60	0.61	0.57	0.53	0.57	0.64	0.63	0.65	0.61	0.62	0.65	0.68	0.67	0.67

0.5m

0.75m

1m

1.25m

Figure 12: Pressure variation with rise height

It is important for Australian Standards to provide accurate wind design data for skillion roofs to ensure structural integrity of the building. Due to the larger suction pressures experienced on the corner region of the top rise eave, a K_L factor of 4.0 is proposed for skillion roof design data. A K_L of 2.5 is proposed on the rise to account for the largest positive and negative pressures occurring as the rise height is increased. Additionally, as AS/NZS 1170.2 does not provide design data for positive pressures on the upwind slope, a C_{fig} value of +0.7 was proposed for the skillion and lean-to roof building.

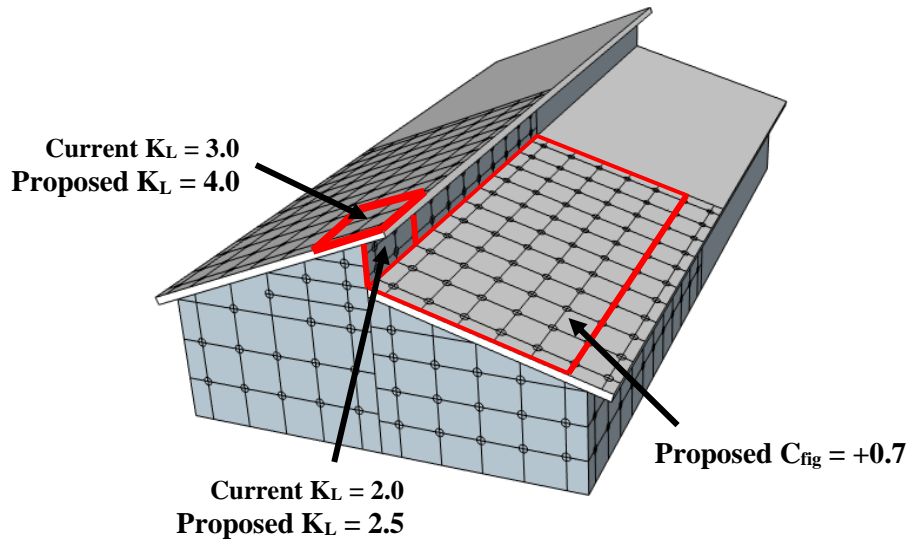


Figure 13: Proposed values for skillion roof design data

4. Conclusions

The external pressures on skillion and lean-to roof buildings were investigated through the use of wind tunnel testing. The rise and upwind slope experienced large positive pressures that corresponded with the largest suction pressures occurring on the corner region of the rise eave. The C_{fig} values found for these regions are larger than the values provided by AS/NZS 1170.2 for related roof slopes. Therefore, proposed for skillion roof design data was a K_L factor of 4.0 for the corner of the rise eave, K_L of 2.5 for the rise, and the addition of positive design data of +0.7 for the upwind slope.

References

- Eaton, J (2020), *Wind Loads on Skillion and Lean-To Roof Buildings*, BE Civil honours thesis, James Cook University, Townsville.
- Standards Australia (2011), *AS/NZS 1170.2: Structural Design Actions Part 2: Wind Loads*, Sydney, Standards Australia.
- Standards Australia (2012), *AS 4055: Wind Loads for Housing*.